East Asian Journal on Applied Mathematics
doi: 10.4208/eajam.300412.200612a

Vol. **2**, No. 3, pp. 185-203
August 2012

A Revisit of the Semi-Adaptive Method for Singular Degenerate Reaction-Diffusion Equations

Qin Sheng[1,*] and A. Q. M. Khaliq[2]

[1] *Department of Mathematics, Center for Astrophysics, Space Physics and Engineering Research, Baylor University, Waco, TX 76798-7328, USA.*
[2] *Department of Mathematical Sciences, Center for Computational Science, Middle Tennessee State University, Murfreesboro, TN 37132, USA.*

Received 30 April 2012; Accepted (in revised version) 20 June 2012

Available online 23 August 2012

Abstract. This article discusses key characteristics of a semi-adaptive finite difference method for solving singular degenerate reaction-diffusion equations. Numerical stability, monotonicity, and convergence are investigated. Numerical experiments illustrate the discussion. The study reconfirms and improves several of our earlier results.

AMS subject classifications: 65M06, 65M12, 65M50, 65Z05, 35K20

Key words: Semi-adaptation, Crank-Nicolson method, quenching singularity, degeneracy, stability, monotonicity, convergence.

1. Introduction

Let $\Omega \subset \mathbb{R}^n$ denote a simply connected finite convex domain, consider a constant $b > 0$, and let u be sufficiently smooth in $\bar{\Omega}$. Many important multiphysics procedures, such as the n-dimensional quenching-combustion process, can be modelled ideally through the following singular reaction-diffusion initial-boundary value problem, or quenching problem:

$$\sigma(x)u_t = \nabla^2 u + f(u), \quad x \in \Omega, \quad t > t_0, \tag{1.1}$$
$$u(x,t) = 0, \qquad x \in \partial\Omega, \ t > t_0, \tag{1.2}$$
$$u(x,t_0) = u_0(x), \qquad x \in \Omega, \tag{1.3}$$

where ∇^2 is the Laplacian, $\partial\Omega$ is the boundary of Ω, $0 \le u_0 \ll b$, and

$$f(0) = f_0 > 0, \qquad f_u(u) > 0, \qquad u \in [0,b), \qquad \lim_{u\to b^-} f(u) = \infty.$$

The degeneracy function $\sigma(x) = 0$ for $x \in \Omega_0 \subset \partial\Omega$ [4,6,10,11].

*Corresponding author. *Email address:* Qin_Sheng@baylor.edu (Q. Sheng)

It has been observed that when the shape of Ω is fixed there exists a critical number $a^* > 0$ such that if a (the n-volume of Ω) is less than a^* then the solution of Eqs. (1.1)–(1.3) exists globally. Otherwise, there exists a finite time $T^*(a)$ such that

$$\lim_{t\to T^*(a)} \sup_{x\in\Omega} u(x,t) = b.$$

Such an a^* is called a *critical value,* T^* a *critical time,* and b the *ignition temperature* [4, 10]. The function u is referred to as a *quenching solution* in the second case. The one-dimensional form of Eqs. (1.1)–(1.3) exhibits a particularly interesting example of the quenching phenomenon when $b = 1$, $\sigma \equiv 1$ and

$$f(u) = \frac{1}{1-u}, \tag{1.4}$$

where the critical value $a^* \approx 1.53045607591062$ [4, 18]. Recent investigations have also revealed that if solutions of Eqs. (1.1)–(1.3) exist they must increase monotonically as t increases at any fixed location $x \in \Omega$ [5, 10, 17].

We address the numerical solution of the one-dimensional form. Without any loss of generality we set $b = 1$ and map a general spatial interval $[s, s+a]$ to $[0,1]$, and consequently consider the dimensionless problem

$$\sigma(x)u_t = \frac{1}{a^2}u_{xx} + f(u), \quad 0 < x < 1, \quad t_0 < t \le T, \tag{1.5}$$

$$u(0,t) = u(1,t) = 0, \qquad t > t_0, \tag{1.6}$$

$$u(x,t_0) = u_0(x), \qquad 0 < x < 1, \tag{1.7}$$

where $T < \infty$ is sufficiently large. The degeneracy and source functions of particular interest in multiphysics applications are

$$\sigma(x) = ax^p(1-x)^{1-p}, \quad f(u) = \frac{1}{(1-u)^q}, \quad 0 \le p \le 1, \quad q > 0, \tag{1.8}$$

for which the following limits are equivalent [5, 18]:

$$\lim_{t\to T_a} \sup_{0<x<1} u(x,t) = 1, \quad \lim_{t\to T_a} \sup_{0<x<1} u_t(x,t) = +\infty \quad \text{whenever } a > a^*.$$

This article is organised as follows. In Section 2 we introduce a second-order Crank-Nicolson scheme for solving Eqs. (1.5)-(1.8), where a uniform spatial mesh is used but adaptive grids controlled by a properly designed arc-length monitoring function are considered in the temporal direction. The structure and approximation is analysed, and both numerical stability in the von Neumann sense and nonlinear error propagation estimates are discussed. Motivated by the desire to preserve the most important physical characteristics of solutions, in Section 3 we focus on the monotonicity and convergence of the numerical solution sequence generated by the semi-adaptive finite difference scheme. Necessary constraints to ensure the correct multiphysical features are obtained, and we remark on the

more general cases. In Section 4, we discuss two computational experiments that validate and illustrate applications of the semi-adaptive algorithm. Important limit values that lead to the occurrence of quenching are carefully estimated, for the particular degeneracy and source functions of interest. Brief concluding remarks are then made in Section 5.

2. Semi-Adaptation and Stability

We rewrite Eqs. (1.5)-(1.8) as

$$u_t = \phi(x)u_{xx} + \psi(x,u), \quad 0 < x < 1, \quad t_0 < t \le T, \tag{2.1}$$
$$u(0,t) = u(1,t) = 0, \qquad t > t_0, \tag{2.2}$$
$$u(x,t_0) = u_0(x), \qquad 0 < x < 1, \tag{2.3}$$

where

$$\phi(x) = \frac{1}{a^2\sigma(x)}, \quad \psi(x,u) = \frac{f(u)}{\sigma(x)} \quad \text{and} \quad T < \infty. \tag{2.4}$$

Let $N \gg 1$ and $\bar{\mathscr{D}}_N = \{x_0, x_1, \cdots, x_{N+1}\}$, $x_k = kh$ be a uniform mesh superimposed over $[0,1]$ with step size $h = 1/(N+1)$. Let $\mathscr{D}_N \subset \bar{\mathscr{D}}_N$ denote the set of interior mesh points. We approximate the spatial derivative in Eq. (2.1) by a second-order central difference — i.e.

$$u_{xx}(x_k,t) \approx \frac{u_{k-1}(t) - 2u_k(t) + u_{k+1}(t)}{h^2}, \qquad x_k \in \mathscr{D}_N.$$

The consequent semidiscretised system from Eqs. (2.1)-(2.3) is thus

$$u' = Au + \psi, \qquad t > t_0, \tag{2.5}$$
$$u(t_0) = u_0, \tag{2.6}$$

where $u = (u_1, u_2, \cdots, u_N)^\top$, $\psi = (\psi_1, \psi_2, \cdots, \psi_N)^\top$, $A = BT \in \mathbb{R}^{N\times N}$,

$$B = \operatorname{diag}\left[\phi_1, \phi_2, \cdots, \phi_N\right], \qquad T = \begin{bmatrix} -2 & 1 & & & \\ 1 & -2 & 1 & & \\ & \cdots & \cdots & \cdots & \\ & & 1 & -2 & 1 \\ & & & 1 & -2 \end{bmatrix},$$

and $\phi_k > 0$, $k = 1, 2, \cdots, N$.

The solution of Eqs. (2.5) and (2.6) exists and is unique if $Au + \psi$ satisfies the Lipschitz condition [8, 11]; and a formal solution of the system is

$$u(t) = E(tA)u_0 + \int_{t_0}^{t} E((t-\tau)A)\psi(u(\tau))d\tau, \qquad t \ge t_0, \tag{2.7}$$

where $E(\cdot) = \exp(\cdot)$ is the matrix exponential.

Lemma 2.1. *All eigenvalues of A are real and negative.*

Proof. Since $A = BT = B^{1/2}B^{1/2}T$, we have $B^{-1/2}A = B^{1/2}T$, whence

$$B^{-1/2}A(B^{1/2})^T = B^{-1/2}AB^{1/2} = B^{1/2}T(B^{1/2})^T$$

because B is diagonal. On the other hand,

$$B^{-1/2}AB^{1/2} = B^{-1/2}BTB^{1/2} = B^{-1/2}B^{1/2}B^{1/2}TB^{1/2} = B^{1/2}TB^{1/2}$$

is symmetric. Thus matrices $B^{-1/2}AB^{1/2}$ and T are congruent. Since the eigenvalues of T are negative and distinct [8, 12], the eigenvalues of $B^{-1/2}AB^{1/2}$ and A must be real and negative, according to Sylvester's law of inertia. □

Lemma 2.2. *For the matrix exponential $E(tA)$,*

$$E(tA) = B^{1/2}E(tB^{1/2}TB^{1/2})B^{-1/2}, \tag{2.8}$$

where $t \in \mathbb{C}$. Further, if $t \in \mathbb{R}^+$ then all eigenvalues of $E(tA)$ are real and $\rho(tA) < 1$, where $\rho(\cdot)$ is the spectral radius of the matrix.

Proof. Since

$$E(tA) = I + tA + \frac{t^2}{2}A^2 + \frac{t^3}{3!}A^3 + \cdots + \frac{t^k}{k!}A^k + \cdots,$$

from Lemma 2.1 we have

$$\begin{aligned}
B^{-1/2}E(tA)B^{1/2} &= B^{-1/2}\left(I + tA + \frac{t^2}{2}A^2 + \frac{t^3}{3!}A^3 + \cdots + \frac{t^k}{k!}A^k + \cdots\right)B^{1/2} \\
&= I + tB^{-1/2}AB^{1/2} + \frac{t^2}{2}B^{-1/2}A^2B^{1/2} + \frac{t^3}{3!}B^{-1/2}A^3B^{1/2} + \cdots \\
&\quad + \frac{t^k}{k!}B^{-1/2}A^kB^{1/2} + \cdots \\
&= I + tB^{-1/2}BTB^{1/2} + \frac{t^2}{2}B^{-1/2}(BT)^2B^{1/2} + \frac{t^3}{3!}B^{-1/2}(BT)^3B^{1/2} + \cdots \\
&\quad + \frac{t^k}{k!}B^{-1/2}(BT)^kB^{1/2} + \cdots \\
&= I + tB^{1/2}TB^{1/2} + \frac{t^2}{2}B^{1/2}TBTB^{1/2} + \frac{t^3}{3!}B^{1/2}TBTBTB^{1/2} + \cdots \\
&\quad + \frac{t^k}{k!}B^{1/2}TBTB\cdots TB^{1/2} + \cdots \\
&= E(tB^{1/2}TB^{1/2}),
\end{aligned}$$

so Eq. (2.8) follows. Further, $tB^{1/2}TB^{1/2}$ is symmetric and all of its eigenvalues are negative and distinct, therefore all eigenvalues of $E(tB^{1/2}TB^{1/2})$ must be of the form $e^{t\lambda}$ where $\lambda < 0$. □

In principle, different numerical quadrature – including the Filon-Levin procedure [21] if the anticipated solution is oscillatory – can be used to solve Eq. (2.7). For instance, the trapezoidal rule yields

$$u(t) \approx E((t-\tau_0)A)u_0 + \frac{t-t_0}{2}\Big[\psi(u(t)) + E((t-t_0)A)\psi(u_0)\Big], \qquad t \geq t_0.$$

Then E can be represented by an appropriately formulated approximation, such as the A-acceptable $1/1$ Padé approximant [1, 12]

$$E(tA) \approx \left(I - \frac{t}{2}A\right)^{-1}\left(I + \frac{t}{2}A\right),$$

to obtain a final numerical solution [5, 12, 14].

Lemma 2.3. *Let $t \in \mathbb{R}^+$. Then*

$$\left\|\left(I - \frac{t}{2}A\right)^{-1}\left(I + \frac{t}{2}A\right)\right\|_2 < \sqrt{\text{cond}(B)} = \sqrt{\frac{\max_k \phi_k}{\min_k \phi_k}}.$$

Proof. Recalling Eq. (2.8), we have

$$\left(I - \frac{t}{2}A\right)^{-1}\left(I + \frac{t}{2}A\right) = B^{1/2}\left(I - \frac{t}{2}B^{1/2}TB^{1/2}\right)^{-1}\left(I + \frac{t}{2}B^{1/2}TB^{1/2}\right)B^{-1/2}.$$

Since $B^{1/2}TB^{1/2}$ is symmetric and all of its eigenvalues are negative and distinct, all eigenvalues of $(I - (t/2)B^{1/2}TB^{1/2})^{-1}(I + (t/2)B^{1/2}TB^{1/2})$ are within $(0, 1)$ [1], hence

$$\begin{aligned}
&\left\|\left(I - \frac{t}{2}A\right)^{-1}\left(I + \frac{t}{2}A\right)\right\|_2 \\
&\leq \left\|B^{1/2}\right\|_2 \times \left\|\left(I - \frac{t}{2}B^{1/2}TB^{1/2}\right)^{-1}\left(I + \frac{t}{2}B^{1/2}TB^{1/2}\right)\right\|_2 \left\|B^{-1/2}\right\|_2 \\
&< \left\|B^{1/2}\right\|_2 \left\|B^{-1/2}\right\|_2 = \sqrt{\text{cond}(B)}.
\end{aligned}$$

□

A highly effective temporal adaptive stepping can be determined via an arc-length procedure [3, 5, 16–20]. Traditionally, the step controller is based on the arc-length of the solution function u. However, in quenching-combustion computations the rate of change function u_t is a far more sensitive choice [5, 17, 18]. Thus we adopt the arc-length monitor function of u_t,

$$m(u_t, t) = \max_x \sqrt{1 + u_{tt}^2}, \qquad t \geq t_0.$$

Let $\tau_j = t_{j+1} - t_j$ denote the variable temporal step. We require consecutive temporal steps to be inversely proportional to corresponding arc-lengths — i.e.

$$\frac{\tau_j}{\tau_{j-1}} = \alpha \frac{\max_x \sqrt{1 + \left(u_{tt}^{(j-1/2)}\right)^2}}{\max_x \sqrt{1 + \left(u_{tt}^{(j+1/2)}\right)^2}}, \qquad \alpha > 0.$$

Values of α between $1/2$ and 2 are traditionally chosen for quenching problems, mainly due to the smoothness concern in equidistribution principals [5,13,18]. In fact, an aggressively large or small proportional constant may lead to a rapid increase of numerical errors [9] or a pollution effect [2], in particular when spatial adaptations are present [3]. We set $\alpha = 1$ for simplicity, and approximate the derivatives by central differences over the intervals $[t_{j-1}, t_j]$ and $[t_j, t_{j+1}]$. Dropping the maximisation notation, we obtain the quadratic relation

$$\tau_j^2 = \tau_{j-1}^2 + \left(u_t^{(j)} - u_t^{(j-1)}\right)^2 - \left(u_t^{(j+1)} - u_t^{(j)}\right)^2, \qquad j = 1, 2, \cdots. \tag{2.9}$$

Theoretically, Eq. (2.9) is sufficient for determining adaptive temporal steps required once τ_0 is given, but in practice it is difficult to use since $u_t^{(j+1)}$ is not known. To overcome this drawback, we may invoke an Euler algorithm

$$u^{(j+1)} \approx w^{(j+1)} = u^{(j)} + \tau_j \left[Au^{(j)} + \psi(u^{(j)})\right] \tag{2.10}$$

or employ a shifted formula

$$\tau_j^2 = \tau_{j-1}^2 + \left(u_t^{(j-1)} - u_t^{(j-2)}\right)^2 - \left(u_t^{(j)} - u_t^{(j-1)}\right)^2, \qquad j = 2, 3 \cdots, \tag{2.11}$$

where τ_0 and τ_1 are given [7,18,20]. However, either way the overall numerical accuracy can be affected.

Quenching phenomena are extremely time sensitive, as can be observed from the rate of change function u_t, which increases faster than exponentially as the quench is approached [4, 10, 11, 16]. This severely limits the application of conventional methods with constant temporal steps, unless the step size used is extremely (even unrealistically) small, for otherwise the numerical results may not represent the correct physical solution. Thus proper semi-adaptations, such as Eqs. (2.9) and (2.11), are frequently the key to the success of a quenching computation. Indeed, spatial adaptations are often considered only after an effective temporal adaptation is adopted [3,14].

Based on the above considerations, we obtain the following semi-adaptive Crank-Nicolson method for solving Eqs. (2.1)-(2.3):

$$u^{(j+1)} = \left(I - \frac{\tau_j}{2}A\right)^{-1} \left(I + \frac{\tau_j}{2}A\right) \left[u^{(j)} + \frac{\tau_j}{2}\psi\left(u^{(j)}\right)\right] + \frac{\tau_j}{2}\psi\left(u^{(j+1)}\right), \tag{2.12}$$

$$u^{(0)} = u_0, \tag{2.13}$$

where τ_j is determined via either (2.9), (2.10) or (2.11). An iterative procedure, or an approximation of the last term in Eq. (2.12), is needed to solve the nonlinear system. Since the high nonlinearity of ψ often leads to multiple solutions of Eqs. (2.12) and (2.13), and upper-lower vectors must be incorporated (cf. [15] and references therein), the second alternative becomes preferable for the computations.

Theorem 2.1. *If the nonlinear function ψ is frozen, then the Crank-Nicolson type method* (2.12)*,* (2.13) *is unconditionally stable in the von Neumann sense.*

Proof. In the linearised case, the perturbation equation corresponding to Eqs. (2.12) and (2.13) is

$$\epsilon^{(j+1)} = \left(I - \frac{\tau_j}{2}A\right)^{-1}\left(I + \frac{\tau_j}{2}A\right)\epsilon^{(j)}, \qquad j \in \{0,1,2,\cdots\},$$

where $\epsilon^{(\ell)} = \tilde{u}^{(\ell)} - u^{(\ell)}$. Advancing continuously, we obtain

$$\epsilon^{(j+m+1)} = \prod_{\ell=j}^{j+m}\left(I - \frac{\tau_\ell}{2}A\right)^{-1}\left(I + \frac{\tau_\ell}{2}A\right)\epsilon^{(j)}, \qquad j \in \{0,1,2,\cdots\}.$$

From Lemma 2.3,

$$\begin{aligned}
\left\|\epsilon^{(j+m+1)}\right\|_2 &\le \left\|\prod_{\ell=j}^{j+m}\left(I - \frac{\tau_\ell}{2}A\right)^{-1}\left(I + \frac{\tau_\ell}{2}A\right)\right\|_2 \left\|\epsilon^{(j)}\right\|_2 \\
&= \left\|\prod_{\ell=j}^{j+m} B^{1/2}\left(I - \frac{\tau_\ell}{2}B^{1/2}TB^{1/2}\right)^{-1}\left(I + \frac{\tau_\ell}{2}B^{1/2}TB^{1/2}\right)B^{-1/2}\right\|_2 \left\|\epsilon^{(j)}\right\|_2 \\
&= \left\|B^{1/2}\left(I - \frac{\tau_{j+m}}{2}B^{1/2}TB^{1/2}\right)^{-1}\left(I + \frac{\tau_{j+m}}{2}B^{1/2}TB^{1/2}\right)\times\cdots\right. \\
&\quad \left.\times\left(I - \frac{\tau_j}{2}B^{1/2}TB^{1/2}\right)^{-1}\left(I + \frac{\tau_j}{2}B^{1/2}TB^{1/2}\right)B^{-1/2}\right\|_2 \left\|\epsilon^{(j)}\right\|_2 \\
&= \left\|B^{1/2}\left[\prod_{\ell=j}^{j+m}\left(I - \frac{\tau_\ell}{2}B^{1/2}TB^{1/2}\right)^{-1}\left(I + \frac{\tau_\ell}{2}B^{1/2}TB^{1/2}\right)\right]B^{-1/2}\right\|_2 \left\|\epsilon^{(j)}\right\|_2 \\
&< \sqrt{\frac{\max_k \phi_k}{\min_k \phi_k}}\left\|\epsilon^{(j)}\right\|_2,
\end{aligned}$$

where the above inequalities hold uniformly for any $m, j \in \{0,1,2,\cdots\}$. The finite difference scheme is thus unconditionally stable in the von Neumann sense. □

Theorem 2.2. *Suppose that the last term in Eq.* (2.12) *is precisely represented during the computation. Then for any initial numerical error* $\epsilon^{(j)}$ *and any nonnegative integers* m *and* j*, an upper bound of the error growth due to Eqs.* (2.12) *and* (2.13) *is*

$$\left\|\epsilon^{(j+m+1)}\right\|_2 < K_{j,m}\sqrt{\mathrm{cond}(B^{1/2})}\left\|\epsilon^{(j)}\right\|_2, \qquad m, j \in \{0,1,2,\cdots\},$$

where

$$K_{j,m} = \prod_{\ell=j}^{m+j}\max_{k=1,\cdots,N} d_k^{(\ell)} \max_{s=1,\cdots,N}\sqrt{d_s^{(j+m+1)}}, \tag{2.14}$$

$$d_k^{(\ell)} = 1 + \frac{q\tau_\ell}{2\left(1 - \xi_k^{(\ell)}\right)^{q+1}\sigma(x_k)}, \qquad 0 < \xi_k^{(\ell)} < 1. \tag{2.15}$$

Proof. Let $\epsilon^{(\ell)} = \tilde{u}^{(\ell)} - u^{(\ell)}$ be the error function due to a perturbation, where $\tilde{u}^{(\ell)}$ denotes the perturbed numerical solution. Note that

$$\psi\left(\tilde{u}^{(\ell)}\right) - \psi\left(u^{(\ell)}\right) = \psi\left(\tilde{u}^{(\ell)}\right) + \psi_u\left(\xi^{(\ell)}\right)\epsilon^{(\ell)} - \psi\left(u^{(\ell)}\right) = \psi_u\left(\xi^{(\ell)}\right)\epsilon^{(\ell)},$$

where $\xi^{(\ell)} \in (\min\{u^{(\ell)}, \tilde{u}^{(\ell)}\}, \max\{u^{(\ell)}, \tilde{u}^{(\ell)}\})$. On the other hand,

$$\psi_u(u) = \frac{f_u(u)}{\sigma(x)} = \frac{q}{(1-u)^{1+q}\sigma(x)} > 0, \qquad x \in (0,1), \quad t > t_0.$$

Thus the perturbation equation for Eqs. (2.12) and (2.13) is

$$\epsilon^{(j+1)} = \left(I - \frac{\tau_j}{2}A\right)^{-1}\left(I + \frac{\tau_j}{2}A\right)D_j\epsilon^{(j)}, \qquad j \in \{0,1,2,\cdots\}, \tag{2.16}$$

where $D_j = \mathrm{diag}(d_1^{(j)}, d_2^{(j)}, \cdots, d_N^{(j)})$ and

$$d_k^{(j)} = 1 + \frac{q\tau_j}{2\left(1-\xi_k^{(j)}\right)^{1+q}\sigma(x_k)} > 1, \qquad k = 1,2,\cdots,N. \tag{2.17}$$

Denoting $D_\ell^{1/2}\epsilon^{(\ell)} = v^{(\ell)}$, we have that Eq. (2.16) can be reformulated as

$$D_{\ell+1}^{-1/2}v^{(j+1)} = \left(I - \frac{\tau_j}{2}A\right)^{-1}\left(I + \frac{\tau_j}{2}A\right)D_j^{1/2}v^{(j)}, \qquad j \in \{0,1,2,\cdots\},$$

hence

$$v^{(j+1)} = D_{j+1}^{1/2}\left(I - \frac{\tau_j}{2}A\right)^{-1}\left(I + \frac{\tau_j}{2}A\right)D_j^{1/2}v^{(j)}, \qquad j \in \{0,1,2,\cdots\}.$$

It follows from Lemma 2.3 that

$$\begin{aligned} v^{(j+m+1)} &= \left[\prod_{\ell=j}^{j+m} D_{\ell+1}^{1/2}\left(I - \frac{\tau_\ell}{2}A\right)^{-1}\left(I + \frac{\tau_\ell}{2}A\right)D_\ell^{1/2}\right]v^{(j)} \\ &= \left[\prod_{\ell=j}^{j+m} D_{\ell+1}^{1/2}B^{1/2}\left(I - \frac{\tau_\ell}{2}B^{1/2}TB^{1/2}\right)^{-1}\left(I + \frac{\tau_\ell}{2}B^{1/2}TB^{1/2}\right)B^{-1/2}D_\ell^{1/2}\right]v^{(j)} \\ &= \left[\prod_{\ell=j}^{j+m} B^{1/2}D_{\ell+1}^{1/2}\left(I - \frac{\tau_\ell}{2}B^{1/2}TB^{1/2}\right)^{-1}\left(I + \frac{\tau_\ell}{2}B^{1/2}TB^{1/2}\right)D_\ell^{1/2}B^{-1/2}\right]v^{(j)}, \end{aligned}$$

which implies that

$$\left\|v^{(j+m+1)}\right\|_2 = \left\|D_{j+m+1}^{1/2}\epsilon^{(j+m+1)}\right\|_2 < K_{j,m}\sqrt{\mathrm{cond}(B^{1/2})}\left\|\epsilon^{(j)}\right\|_2, \tag{2.18}$$

where

$$K_{j,m} = \left\| D_{j+m+1}^{1/2} \right\|_2 \prod_{\ell=j}^{m+j} \left\| D_{j+m+1}^{1/2} \right\|_2^2 = \prod_{\ell=j}^{m+j} \max_{k=1,..,N} d_k^{(\ell)} \sqrt{\max_{s=1,..,N} d_s^{(j+m+1)}}.$$

Combining Eqs. (2.17) and (2.18), we obtain

$$\left\| \epsilon^{(j+m+1)} \right\|_2 < K_{j,m} \sqrt{\mathrm{cond}(B^{1/2})} \left\| \epsilon^{(j)} \right\|_2, \qquad m, j \in \{0, 1, 2, \cdots\}. \qquad \square$$

Remark 2.1. Theorem 2.1 demonstrates the linear stability of Eqs. (2.12) and (2.13) when nonlinearity is neglected and the numerical stability is considered locally within a small neighbourhood of $t_j = \sum_{\ell=1}^{j} \tau_\ell + t_0$. It has been found that this consideration is extremely valuable and useful, especially for real world applications [5, 18, 20]. The role of the quenching nonlinearity on the stability is defined by Theorem 2.2, which gives an effective upper bound on the error propagation. Although the overall stability in the classical sense cannot be guaranteed, this provides a suitable way to evaluate the accuracy and reliability of the underlying nonlinear difference scheme of Eqs. (2.12) and (2.13).

Remark 2.2. Apparently, the coefficient $K_{j,m}$ plays a particularly important role in the error bound given by Theorem 2.2. The magnitude of $K_{j,m}$ depends on the arc-length feature of the semi-adaptation. When $\xi_k^{(\ell)} \to 1^-$ we have $\tau_\ell \to 0$ and consequently $d_k^{(\ell)} \to 1$, so the growth in the magnitude of of $K_{j,m}$ may slow down significantly as the numerical solution approaches quenching. This observation is validated in our computational experiments discussed below.

Remark 2.3. All of the above results are valid if Eq. (2.2) is replaced by the nonhomogeneous boundary conditions

$$u(0,t) = c(t), \qquad u(1,t) = d(t), \qquad t > t_0,$$

when $0 \le c,\ d \ll 1$. A nonuniform adaptive mesh in space can also be incorporated to achieve better approximate solutions of the singular problem (2.1)–(2.3), but may significantly increase the level of difficulty in the subsequent analysis. Refs. [8, 9, 14] and references therein provide details of nonuniform finite difference formulations. Compact scheme techniques can also be convenient for the problem.

3. Monotonicity and Convergence

As discussed extensively in Refs. [5,16–19], matrix positivity and solution vector monotonicity are among the most distinctive characteristics of singular reaction-diffusion equations such as Eqs. (1.1)–(1.3) and Eqs. (2.1)–(2.3). These properties reflect the proper natural behaviour of the multiphysical processes modelled by the underlying differential

equations, so it is crucial for the numerical solution to preserve and reflect such key characteristics [4, 6, 13].

Let us denote $\phi_{\min} = \min_{k=1,2,\ldots,N} \phi_k$ and $\phi_{\max} = \max_{k=1,2,\ldots,N} \phi_k$. Further, let $\vee$ denote one of the operations $<, \leq, >, \geq$; and for $\alpha, \beta \in \mathbb{R}^N$ we adopt the following notation:

1. $\alpha \vee \beta$ means $\alpha_k \vee \beta_k$, $k = 1, 2, \cdots, N$;
2. $c \vee \alpha$ means $c \vee \alpha_k$, $k = 1, 2, \cdots, N$, for any $c \in \mathbb{R}$.

Assume the Courant number $\gamma_j = \tau_j/h^2 \leq a^2\phi_{\min}$. It can be verified that $d_k^{(0)} < 2$, $k \in \{1, 2, \cdots\}$, $\psi\left(u^{(0)}\right) \geq 0$ and $u^{(1)} < 1$ if $u^{(0)} \equiv 0$ [5, 16–19].

Lemma 3.1. *If $\tau_j\phi_{\max} < 1$, $j \in \{1, 2, \cdots\}$ then both $I - (\tau_j/2)A$ and $I + (\tau_j/2)A$ are nonsingular. Further, $I+(\tau_j/2)A$ is nonnegative, $I-(\tau_j/2)A$ is monotone and inverse-positive, and $I + (\tau_j/2)A$ is nonnegative.*

Proof. The conclusions are straightforward, due to the particular structure of the matrix $A = BT$ [12, 16]. □

Lemma 3.2. *Let $\tau_j\phi_{\max} < 1$, $j \in \{1, 2, \cdots\}$. If there exists $\ell > 0$ such that*

(i) $d_k^{(j)} \leq 2$ $k = 1, 2, \cdots, N$, $j = 0, 1, \cdots, \ell$, *and*
(ii) $Au^{(j)} + \psi\left(u^{(j)}\right) \geq 0$, $j = 0, 1, \cdots, \ell$,

then the solution sequence $u^{(0)}$, $u^{(1)}$, $\cdots$, $u^{(\ell)}$, $\cdots$ is monotonically increasing.

Proof. From Eq. (2.12) we have

$$\begin{aligned} u^{(j+1)} - u^{(j)} &= \left(I - \frac{\tau_j}{2}A\right)^{-1}\left(I + \frac{\tau_j}{2}A\right)\left[u^{(j)} + \frac{\tau_j}{2}\psi\left(u^{(j)}\right)\right] \\ &\quad + \frac{\tau_j}{2}\psi\left(u^{(j+1)}\right) - u^{(j)} = \left(I - \frac{\tau_j}{2}A\right)^{-1} v^{(j)}, \end{aligned} \tag{3.1}$$

where

$$\begin{aligned} v^{(j)} &= \left(I + \frac{\tau_j}{2}A\right)\left[u^{(j)} + \frac{\tau_j}{2}\psi\left(u^{(j)}\right)\right] - \left(I - \frac{\tau_j}{2}A\right)\left[u^{(j)} - \frac{\tau_j}{2}\psi\left(u^{(j+1)}\right)\right] \\ &= \tau_j Au^{(j)} + \frac{\tau_j}{2}\left(I + \frac{\tau_j}{2}A\right)\psi\left(u^{(j)}\right) + \frac{\tau_j}{2}\left(I - \frac{\tau_j}{2}A\right)\psi\left(u^{(j+1)}\right) \\ &= \tau_j Au^{(j)} + \tau_j\psi\left(u^{(j)}\right) + \frac{\tau_j}{2}\left(I - \frac{\tau_j}{2}A\right)\psi_u\left(\xi^{(j)}\right)\left(u^{(j+1)} - u^{(j)}\right), \end{aligned}$$

so Eq. (3.1) yields

$$\left[I - \frac{\tau_j}{2}\psi_u\left(xi^{(j)}\right)\right]\left(u^{(j+1)} - u^{(j)}\right) = \tau_j\left(I - \frac{\tau_j}{2}A\right)^{-1}\left[Au^{(j)} + \psi\left(u^{(j)}\right)\right]$$

and hence

$$u^{(j+1)}-u^{(j)}=\tau_j\left[I-\frac{\tau_j}{2}\psi_u\left(xi^{(j)}\right)\right]^{-1}\left(I-\frac{\tau_j}{2}A\right)^{-1}\left[Au^{(j)}+\psi\left(u^{(j)}\right)\right].$$

From Eq. (2.17), the nonzero elements of the diagonal matrix $I-(\tau_j/2)\psi_u\left(xi^{(j)}\right)$ are

$$2-d_k^{(j)}\geq 0,\qquad k=1,2,\cdots,N$$

due to (ii), so $[I-(\tau_j/2)\psi_u(xi^{(j)})]^{-1}$ is nonnegative such that $u^{(j+1)}-u^{(j)}\geq 0$. □

Theorem 3.1. *Suppose that the following inequality holds:*

$$\max_k\frac{\sqrt{\phi_k}}{\left|2-d_k^{(j)}\right|}\max_s\frac{d_s^{(j+1)}}{\sqrt{\phi_s}}\ \leq\ 1.$$

Then the semi-adaptive method (2.12) *and* (2.13) *is convergent.*

Proof. Similar to the discussion of the key characteristics of the trapezoidal method in Ref. [8], if $U_k^{(\ell)}$ is the exact solution of Eqs. (2.1)–(2.3) then

$$U^{(j+1)}=\left(I-\frac{\tau_j}{2}A\right)^{-1}\left(I+\frac{\tau_j}{2}A\right)\left[U^{(j)}+\frac{\tau_j}{2}\psi\left(U^{(j)}\right)\right]+\frac{\tau_j}{2}\psi\left(U^{(j+1)}\right)+O\left(\tau_j^2\right).$$

Subtracting Eq. (2.12) and denoting $\varepsilon^{(\ell)}=U^{(j+1)}-u^{(j+1)}$, it follows that

$$\begin{aligned}\varepsilon^{(j+1)}=&\left(I-\frac{\tau_j}{2}A\right)^{-1}\left(I+\frac{\tau_j}{2}A\right)\left\{\varepsilon^{(j)}+\frac{\tau_j}{2}\left[\psi\left(U^{(j)}\right)-\psi\left(u^{(j)}\right)\right]\right\}\\&+\frac{\tau_j}{2}\left[\psi\left(U^{(j+1)}\right)-\psi\left(u^{(j+1)}\right)\right]+O\left(\tau_j^2\right).\end{aligned}\tag{3.2}$$

Note that

$$\psi\left(U^{(\ell)}\right)-\psi\left(u^{(\ell)}\right)=\psi_u\left(\xi^{(\ell)}\right)\varepsilon^{(\ell)},$$

where $\xi^{(\ell)}$, $\xi_k^{(\ell)}\in(\min\{u_k^{(\ell)},U_k^{(\ell)}\},\ \max\{u_k^{(\ell)},U_k^{(\ell)}\})$, $k=1,2,\cdots,N$. Recalling Eq. (2.17), from Eq. (3.2) we obtain

$$\varepsilon^{(j+1)}=\left(I-\frac{\tau_j}{2}A\right)^{-1}\left(I+\frac{\tau_j}{2}A\right)D_j\varepsilon^{(j)}+(D_{j+1}-I)\varepsilon^{(j+1)}+O\left(\tau_j^2\right),$$

so that

$$(2I-D_{j+1})\varepsilon^{(j+1)}=\left(I-\frac{\tau_j}{2}A\right)^{-1}\left(I+\frac{\tau_j}{2}A\right)D_j\varepsilon^{(j)}+O\left(\tau_j^2\right).$$

Denoting

$$\begin{aligned}M_j=&(2I-D_{j+1})^{-1}\left(I-\frac{\tau_j}{2}A\right)^{-1}\left(I+\frac{\tau_j}{2}A\right)D_j\\=&(2I-D_{j+1})^{-1}B^{1/2}\left(I-\frac{t}{2}B^{1/2}TB^{1/2}\right)^{-1}\left(I+\frac{t}{2}B^{1/2}TB^{1/2}\right)B^{-1/2}D_j,\end{aligned}$$

we have

$$\begin{aligned}\left\|M_j\right\|_2 &< \left\|(2I - D_{j+1})^{-1}B^{1/2}\right\|_2 \left\|B^{-1/2}D_j\right\|_2 \\ &= \max_k \frac{\sqrt{\phi_k}}{\left|2 - d_k^{(j)}\right|} \max_s \frac{d_s^{(j+1)}}{\sqrt{\phi_s}} \ \leq \ 1\end{aligned}$$

such that

$$\left\|\varepsilon^{(j+1)}\right\|_2 = \left\|M_j\varepsilon^{(j)} + O\left(\tau_j^2\right)\right\|_2 < \left\|\varepsilon^{(j)}\right\|_2 + C\tau_j^2,$$

where $C_j > 0$. Using the above inequality recursively, we obtain

$$\begin{aligned}\left\|\varepsilon^{(j+1)}\right\|_2 &< \left\|\varepsilon^{(j-1)}\right\|_2 + C\tau_{j-1}^2 + C\tau_j^2 \\ &= \left\|\varepsilon^{(0)}\right\|_2 + C\tau_0^2 + C\tau_1^2 + \cdots + C\tau_{j-1}^2 + C\tau_j^2 \\ &= C\tau_0^2 + C\tau_1^2 + \cdots + C\tau_{j-1}^2 + C\tau_j^2,\end{aligned}$$

since $\varepsilon^{(0)} = 0$ due to the initial value used. Let $\tau = \max_\ell \tau_\ell \ll 1$ and hence

$$\left\|\varepsilon^{(j+1)}\right\|_2 < C\tau\left(\tau_0 + \tau_1 + \cdots + \tau_j\right) \leq CT\tau,$$

so that

$$\lim_{h,\tau\to 0}\left\|\varepsilon^{(j+1)}\right\|_2 = 0$$

ensures the anticipated convergence. □

We also readily obtain the following Theorem.

Theorem 3.2. *For any beginning solution* $u^{(\ell)} < 1,\ \ell \geq 1$, *if*

(i) $\gamma_j = \tau_j/h^2 \leq a^2\phi_{\min}$,
(ii) $d_k^{(j)} \leq 2,\ k = 1, 2, \cdots, N,$ *and*
(iii) $Au^{(j)} + \psi(u^{(j)}) \geq 0$

where $j = \ell,\ \ell+1, \ell+2, \cdots$, *then the solution vector sequence* $u^{(\ell)}$, $u^{(\ell+1)}$, $u^{(\ell+2)}, \cdots$ *produced by the semi-adaptive scheme* (2.12) *and* (2.13) *increases monotonically until unity is exceeded by a component of the vector (i.e. until quenching occurs) or converges to the steady solution of the problem (when there is no quenching solution).*

Proof. The proof can be viewed as a straightforward simplification of the proofs for similar results in the two-dimensional context [5, 16, 18]. □

Remark 3.1. We note that condition (iii) of Theorem 3.2 is ensured at least for the case $\ell = 0$ and $u^{(0)}$. It seems that the solution monotonicity requires more rigorous constraints than for numerical stability and convergence, as an additional numerical feature definitely justified for expected quenching phenomena, but the monotonicity requirement has also made applications of nonuniform spatial grids difficult.

4. Numerical Experiments and Conclusions

Numerical experiments have validated results presented in Refs. [16-19], where similar differential equation structures are considered. Since our computational procedures are similar, there is little need to repeat most standard data, figures and simulations — so we only illustrate key features of solutions of the singular reaction-diffusion equation involving new and different degenerate functions in Eq. (1.8). To this end, we consider the following nonlinear initial-boundary value problem:

$$ax^p(1-x)^{1-p}u_t = \frac{1}{a^2}u_{xx} + \frac{1}{(1-u)^q}, \qquad 0<x<1, \quad t_0<t\le T, \tag{4.1}$$

$$u(0,t) = u(1,t) = 0, \qquad t > t_0, \tag{4.2}$$

$$u(x,t_0) = u_0(x), \qquad 0<x<1, \tag{4.3}$$

with the parameters $0 \le p \le 1$ and $q > 0$.

Without loss of generality, we set $q = 1$ and let the temporal adaptation start when $v(t) = \max_{0\le x\le 1} u(x,t)$ reaches a certain value, say, $v^* = 0.95$. For different values of a, possible corresponding quenching time and locations are searched and confirmed to exist. Our second-order semi-adaptive algorithm (2.12) and (2.13) is found to be extremely easy and reliable to use. The variable t-step generator is effective and accurate. Courant numbers used for the implicit scheme are around unity. All programs are either implemented using FORTRAN 95 with desirable NAG subroutines or MATLAB-SIMULINK packages.

For programming purposes, we re-write Eq. (2.12) as

$$\left(I - \frac{\tau_j}{2}A\right)u^{(j+1)} = \left(I + \frac{\tau_j}{2}A\right)u^{(j)} + g\left(u^{(j)}, w^{(j+1)}\right), \qquad j = 0,1,\cdots,$$

where

$$g\left(u^{(j)}, w^{(j+1)}\right) = \frac{\tau_j}{2}\left[\left(I + \frac{\tau_j}{2}A\right)\psi\left(u^{(j)}\right) + \left(I - \frac{\tau_j}{2}A\right)\psi\left(w^{(j+1)}\right)\right]$$

and $w^{(j+1)}$ is determined by Eq. (2.10). We consider homogeneous Dirichlet boundary conditions and the smooth initial data function

$$u_0(x) = \mu \sin\frac{\pi x}{a}, \qquad 0 \le x \le a, \quad 0 \le \mu \ll 1.$$

Case I: no quenching, when $a = 1$ and $\mu = 0.001,\ 0.005$.

The solution u on Fig. 1 increases monotonically and the rate of change u_t decreases continuously as t increases, so u becomes extremely smooth and flat, with a maximum value $u^* \approx 0.141830 \ll 1$. Although the degeneracy plays a significant role in disturbances during the initial stage of the computations, strong diffusion dominates in later stages. These features are seen more clearly in Figs. 2 and 3, where three-dimensional views of the u, u_t are given. Solution surfaces are locally enlarged. The phenomena demonstrated are consistent with theoretical predictions [4, 6, 10].

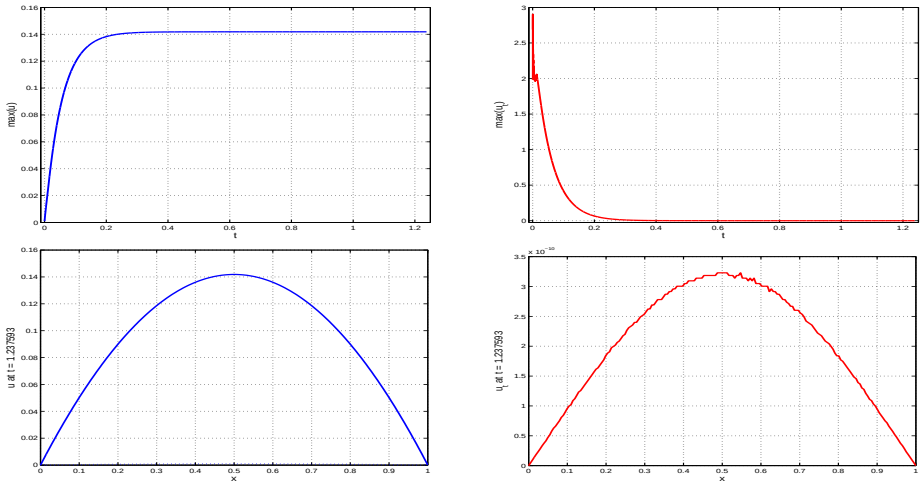

Figure 1: Profiles of the solution u (blue) and u_t (red). TOP: $\max_x u$ and $\max_x u_t$ as t increases. BOTTOM: u and u_t at the end of experiments. Up to 200,000 temporal steps are executed. Adaptation has never been activated due to flat u_t values. No quenching solution is observed.

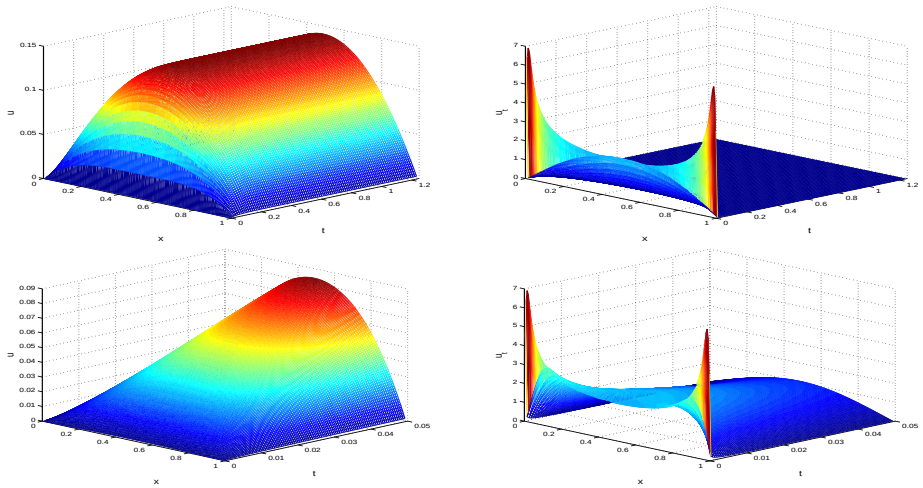

Figure 2: Three-dimensional views of u and u_t. TOP: Plots for $t \in [0, 1.2376]$. BOTTOM: Locally enlarged plots for the beginning stage of $t \in [0, 0.0495]$. Impacts of the degenerate singularity can clearly be seen.

The first 200 solutions of Eqs. (4.1)–(4.3) in the sequence with $p = 1/5$ are shown in Fig. 3. An intensive degeneracy effect can be observed near $x = a$. Although solution surfaces swing toward $x = 1$ initially, they quickly come back to normal symmetry afterward. In other words, when the solution values are relatively small (i.e. when t is relatively small), the degeneracy does contribute to both u and u_t significantly. However, as the solutions evolve and stronger diffusion starts to kick in, the degeneracy is quickly smoothed out. Thus the influence of degeneracy on the numerical solutions is local and limited, and the degeneracy may almost be neglected in later stages of the quenching computations.

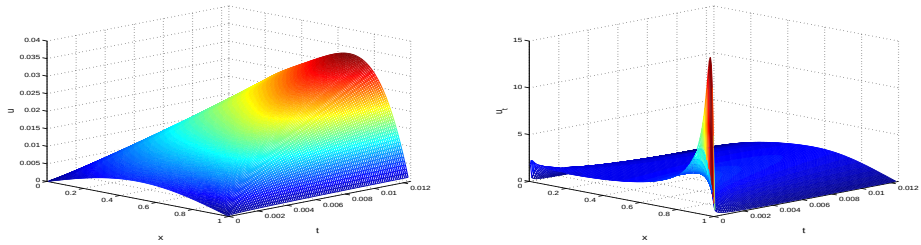

Figure 3: Three-dimensional views of u and u_t in the first 200 temporal steps ($0 \le t \le 0.012326$). Parameter values $p = 0.2$ and $\mu = 0.005$ are used. A large disturbance can be observed in the beginning stage at $x = 1$, although it rapidly vanishes later on. The numerical solutions are not symmetric with respect to $x = a/2$ at first, but they recover very quickly to symmetric solutions.

Case II: quenching, when $a = \pi$ and $\mu = 0.001$.

We present profiles of u and u_t in Fig. 4. Unlike Case I, a strong quenching singularity now occurs. As soon as the time t approaches $T_\pi^* \approx 0.792907811312324$, u quenches and u_t blows up simultaneously. The adaptation is activated at $\max_x u = 0.95$ and then remains throughout the computations. To clearly illustrate the characteristic structures and features of the solutions, in Fig. 5 we show three-dimensional surfaces of both u and u_t in the final 50 steps before the quenching. It is observed that while u approaches the unity in the center of the spatial domain smoothly, u_t blows up violently at the quenching time T_π^*. The interesting phenomena are again consistent with theoretical predictions and our previous investigations [16, 17, 19].

The influence of the degeneracy is continuous in this case. To illustrate this, we show more details of the solutions in Fig. 6 for $p = 0.5$, where the initial 120 temporal steps are displayed. The degeneracy contributions are significant near both ends of the spatial interval. In Fig. 7 where $p = 0.66$, the solutions of Eqs. (4.1)–(4.3) are displayed for the initial 2,000 temporal steps, and it can again be seen that the degeneracy contributions are significant near the ends of the spatial interval. We also show the last 80 solutions immediately before the quenching. Probably due to the strong diffusion features of the differential equation and the numerical stability of the semi-adaptive method (2.12) and (2.13), the degeneracy disturbances at the endpoints diminish as the solution advances. We also find the degeneracy does affect the solution symmetry. Thus in the last row of the Figures, the numerical solutions are apparently pushed toward $x = 0$ by the stronger degeneracy at $x = 0$, and consequently the quenching location is slightly shifted to $x^* \approx 1.203495693166239$.

To further illustrate the influence of degeneracy on the quenching singularity, the numerical solution u immediately before quenching is shown in Fig. 8 where different p values are employed. Detailed information about the quenching time and location is given in Table 1. It is interesting to observe that the quenching location is not a simple linear function of p.

Finally, in Table 2 we give transitional extreme values of u and u_t across the quenching time T_π^*. An artificial singularity remover is used to secure the source function during the computations. It is anticipated that values of u decline when the source function becomes

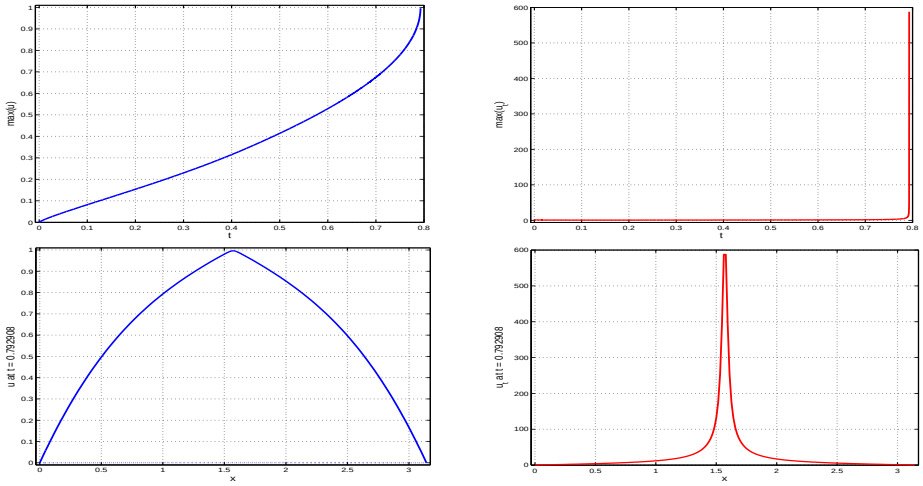

Figure 4: Profiles of solution u (blue) and u_t (red). $p = 0.5$ is used. TOP: $\max_x u$ and $\max_x u_t$ as t increases. BOTTOM: u and u_t immediately before the quenching. Up to 12,983 temporal steps are executed. Adaptation kicks in at $\max_x u \approx 0.95$ and remains throughout the rest of the calculations. The quenching solution is observed until the quenching time $T_\pi^* \approx 0.792907811312324$.

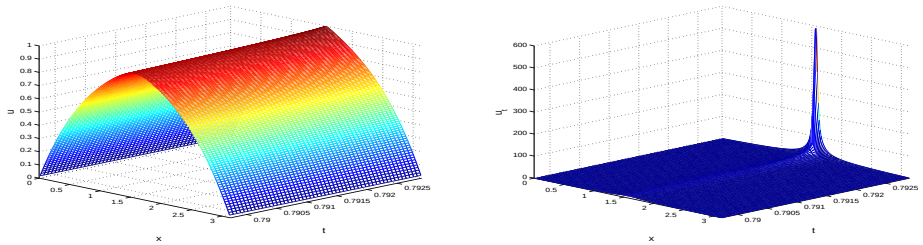

Figure 5: Three-dimensional views of u and u_t in the final 50 temporal steps before the quenching ($0.789732 \le t \le 0.792907$). The peak value of u_t is approximately 587.781919. Quenching is observed.

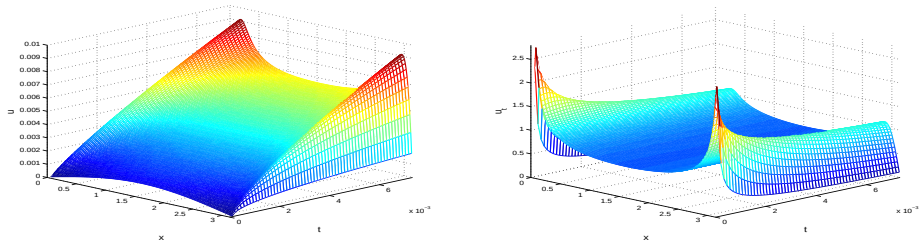

Figure 6: Three-dimensional views of u and u_t in the first 120 temporal steps ($0 \le t \le 0.007329$). Peak value of $u_t \approx 2.741833$. The degenerate singularity near the end points is visible.

negative, and this is clearly reflected in the Table. This also raises the issue of the post-quenching mechanism [11, 14, 18], and a more rigorous numerical study is desirable to investigate that.

To conclude, in this article we have reconsidered a semi-adaptive finite difference method for solving a degenerate singular reaction-diffusion partial differential equation problem. The one-dimensional nonlinear equation is closely related to multiphysical appli-

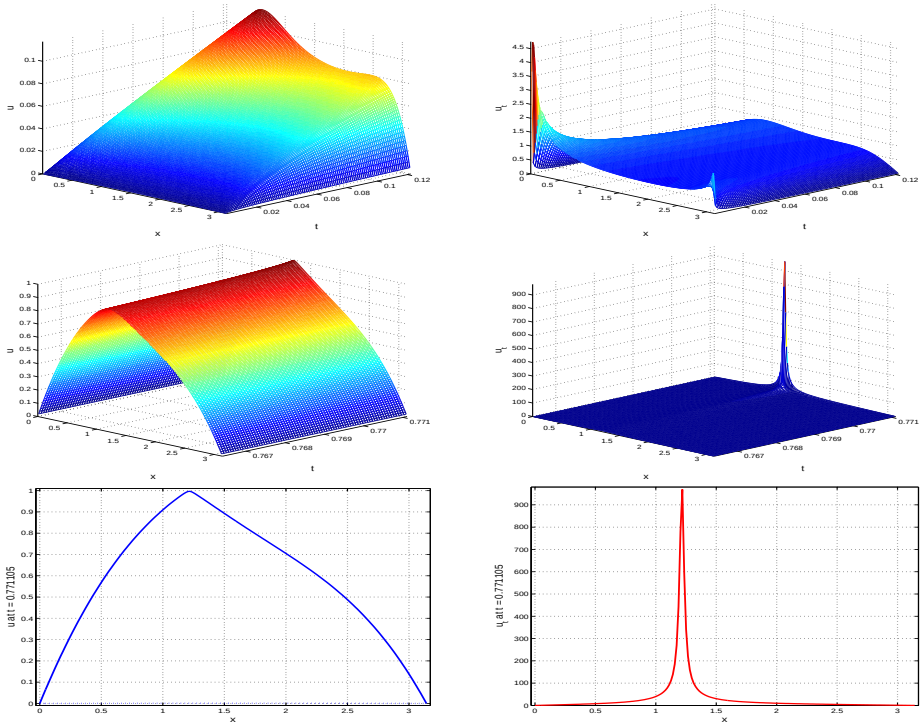

Figure 7: Profiles of solution u (blue) and u_t (red) with $a = \pi$, $p = 0.66$ and $\mu = 0.01$. TOP: The first 2,000 $\max_x u$ and $\max_x u_t$. MIDDLE: The last 80 solutions. BOTTOM: u and u_t at the end of experiments. Up to 12,626 temporal steps are executed. Adaptation kicks in once $\max_x u \geq 0.95$. The quenching solution is observed with a quenching time $T_\pi^* \approx 0.771104831366368$.

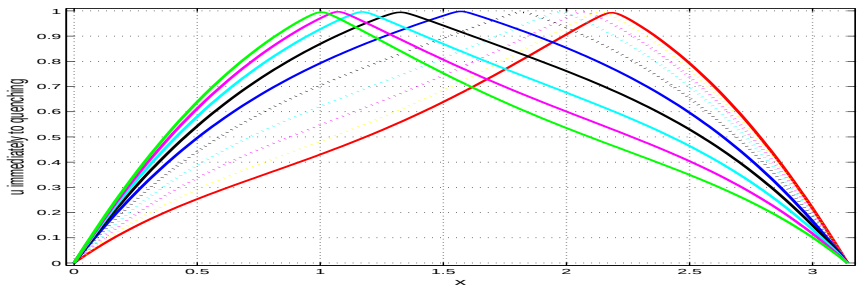

Figure 8: Profiles of the solution u immediately before quenching. Parameters $a = \pi$, $\mu = 0.055$ are used. Curves with peaks from the left to right are for $p = 0.9, 0.8, 0.7, 0.6, 0.5, 0.4, 0.3, 0.2, 0.1$ and 0.01, respectively. Apparently, there are four symmetric pairs of curves with respect to the line $x = \pi/2$ due to the particular structure of σ given in (1.8).

cations, in particular to quenching-combustion and oil pipeline decay predictions [4]. An improved analysis of key issues has been made — including the stability, monotonicity, and convergence of the numerical scheme. Simulation experiments not only demonstrate the singular numerical solutions, but also the degeneracy and quenching point singularities.

The numerical method studied uses a uniform spatial mesh. Spatial adaptations may reduce the overall accuracy of a finite difference method if the algorithmic simplicity needs

Table 1: Quenching time T_π^* and location x_π^* when different p values are used in the degeneracy function. Parameters used are the same as in Fig. 8. It is observed that while the p value increases, the quenching time increases and the quenching location decreases for $p \in (0, 0.5]$.

p	T_π^*	x_π^*
0.01	0.609506274119872	2.188173987574980
0.1	0.639615151188096	2.141284544984088
0.2	0.671678356990973	2.063135473999267
0.3	0.700321487508209	1.969356588817482
0.4	0.722063394681207	1.813058446847841
0.5	0.730884483378537	1.562981419696415

Table 2: Extreme values of u and u_t across the quenching time T_π^*. An artificial remover of the singular points of the source function is adopted. The u values decline almost immediately after the quenching time due to the negative values of u_t and the source term. Parameters $a = \pi$, $p = 0.66$ and $\mu = 0.001$ are used. The temporal step is fixed throughout these calculations.

t	$\max_{0\le x\le\pi} u(x,t)$	$\text{extreme}_{0\le x\le\pi} u_t(x,t)$
0.771043758593411	0.996877873302507	78.303318541261902
0.771104831366368	1.008759826535204	194.5540157622561
0.771117099081744	1.005801097883084	-241.1800862263735
0.771120372019206	1.004127237184930	-511.4245896057617
0.771123644956668	1.002776752452407	-412.6216123365225
0.771126917894129	1.001543546874073	-376.7886165763463
0.771130190831591	0.998547291992905	-915.4635296984035
0.771130408549460	0.997632562002846	-420.1446551479296

to be preserved [9], but in future we intend to provide an optimised balance between spatial adaptation and efficiency in singular reaction-diffusion equation computations.

There are many other important and interesting computational issues related to singular problems such as (1.1)–(1.3), (1.5)–(1.7), (2.1)–(2.3) and (4.1)–(4.3). The open issues include the use of nonlocal boundary conditions, coupled equations with distinctive singular features, nonlinear degeneracy impact to the quenching, and numerical impulsive quenching for highly effective fuel combustion designs. This article is intended to promote further research in the promising field.

Acknowledgments

The first author is supported in part by the URC research grants (No. 30-330119-11 and 18-330107-12) from the Baylor University. We would like to thank the anonymous referees for their valuable input, which enhanced the quality and presentation of this paper.

References

[1] G. A. Baker and A. Graves-Morris, *Padé Approximants,* Cambridge University Press, London and New York, 1995.

[2] G. Bao, G. W. Wei and S. Zhao, Numerical solution of the Helmholtz equation with high wavenumbers, *Int. J. Numer. Meth. Engng.,* **59** (2004), 389–408.
[3] M. Beauregard and Q. Sheng, Solving degenerate quenching-combustion equations by an adaptive splitting method on evolving grids, *Computers Struct.,* (2012), in press.
[4] C. Y. Chan and L. Ke, Parabolic quenching for nonsmooth convex domains, *J. Math. Anal. Appl.,* **186** (1994), 52–65.
[5] H. Cheng, P. Lin, Q. Sheng and R. C. E. Tan, Solving degenerate reaction-diffusion equations via variable step Peaceman-Rachford splitting, *SIAM J. Sci. Comput.,* **25** (2003), 1273–1292.
[6] P. Ferreira, Numerical quenching for the semilinear heat equation with a singular absorption, *J. Comput. Appl. Math.,* **228** (2009), 92–103.
[7] R. M. Furzeland, J. G. Verwer and P. A. Zegeling, A numerical study of three moving-grid methods for one-dimensional partial differential equations which are based on the method of lines, *J. Comput. Phys.,* **89** (1990), 349–388.
[8] A. Iserles, *A First Course in the Numerical Analysis of Differential Equations,* Cambridge University Press, 2nd Ed., New York, 2011.
[9] B. Jain and A. Sheng, An exploration of the approximation of derivative functions via finite differences, *Rose-Hulman Undergrd. Math J.,* **8** (2007), 172–188.
[10] H. Levine, Quenching, nonquenching, and beyond quenching for solutions of some parabolic equations, *Ann. Math. Pure Appl.,* **4** (1989), 243–260.
[11] N. Nouaili, A Liouville theorem for a heat equation and applications for quenching, *Nonlinearity,* **24** (2011), 797–832.
[12] G. Poole and T. Boullion, A survey on M-matrices, *SIAM Review,* **16** (1974), 419–427.
[13] Z. Qiao, Z. Zhang and T. Tang, An adaptive time-stepping strategy for the molecular beam epitaxy models, *SIAM J. Sci. Comput.,* **33** (2011), 1395–1414.
[14] Q. Sheng, Adaptive decomposition finite difference methods for solving singular problems, *Frontiers Math. China,* **4** (2009), 599–626.
[15] Q. Sheng and R. Agarwal, Nonlinear variation of parameter methods for summary difference equations in several independent variables, *J. Appl. Math. Comput.,* **61** (1994), 39-60.
[16] Q. Sheng and H. Cheng, An adaptive grid method for degenerate semilinear quenching problems, *Computers Math. Appl.,* **39** (2000), 57–71.
[17] Q. Sheng and A. Q. M. Khaliq, A compound adaptive approach to degenerate nonlinear quenching problems, *Numer. Meth. Partial Diff. Eqns,* **15** (1999), 29–47.
[18] Q. Sheng and A. Q. M. Khaliq, Linearly implicit adaptive schemes for singular reaction-diffusion equations, Chapter 9, *Adaptive Method of Lines,* CRC Press, London and New York, 2001.
[19] Q. Sheng and A. Q. M. Khaliq, Modified arc-length adaptive algorithms for degenerate reaction-diffusion equations, *Appl. Math. Comput.,* **126** (2002), 279–297.
[20] Z. J. Tan, Z. R. Zhang, Y. Q. Huang and T. Tang, Moving mesh methods with locally varying time steps, *J. Comput. Phys.,* **200** (2004), 347–367.
[21] J. Trevelyan and M. E. Honnor, A numerical coordinate transformation for efficient evaluation of oscillatory integrals over wave boundary elements, *J. Integ. Eqn,* **21** (2009), 447–468.